Research Article

Israel Journal of Chemistry
www.ijc.wiley-vch.de

doi.org/10.1002/ijch.202300006

Practical Aspects of Thermal Dissociation and Recombination Reactions: The Reaction Systems $CF_3X(+M) \leftrightarrow CF_3 + X\ (+M)$ with X = F, Cl, Br, and I

Carlos Jorge Cobos,[a] Elsa Tellbach,[b] Lars Sölter,[b] and Jürgen Troe*[b]

Dedicated to Prof. Helmut Schwarz on the occasion of his 80th birthday

Abstract: The thermal dissociation/recombination reactions of the perfluoromethyl halides $CF_4 \leftrightarrow CF_3 + F$, $CF_3Cl \leftrightarrow CF_3 + Cl$, $CF_3Br \leftrightarrow CF_3 + Br$, and $CF_3I \leftrightarrow CF_3 + I$ are analyzed with respect to their transition (for increasing pressures) from second-order to first-order dissociation (or from third-order to second-order recombination). The dependence of this transition on the temperature is documented. Practical aspects of the modelling of falloff curves are discussed.

1. Introduction

For over one hundred years,[1] the rate constants of thermal dissociation (and the reverse recombination) reactions have been interpreted as a competition between intermolecular collisional activation (and deactivation) and intramolecular rearrangement processes. The consequence of this competition are pressure- (or bath gas concentration [M]-) dependent rate "constants", i. e. the falloff curves of the reactions. Information on these curves is of considerable fundamental as well as practical importance. On the one hand, the measured rate constants may provide information on molecular properties of the reacting species. On the other hand, temperature- and pressure-dependences of rate constants are required for a quantitative modelling of numerous phenomena governed by reaction kinetics, such as combustion, atmospheric, or interstellar chemistry.[2–4]

Over the past about 15 years, our group has combined experimental studies of thermal dissociation reactions of fluorocarbons with theoretical treatments based on statistical unimolecular rate theories in combination with quantum-chemical calculations. The results allowed us to represent pressure- and temperature-dependences of rate constants in a compact manner and over wide ranges of conditions. Allowing for an adjustment of few, only incompletely known, molecular parameters at some place of the available experiments, the modelled rate constants then could be extrapolated into ranges which are not easily accessible experimentally. The present article illustrates this for the series of perfluoromethyl halides which so far have been studied only to a limited extent. Reactions of this class of molecules may be of practical importance, e. g., in the search for SF_6-alternative substances, having smaller global warming potential than SF_6 and being useful as insulation and arc-suppressing gases in high-pressure electrical switches.[5–7] In addition, such reactions may also be important for the modelling of plasma etching processes, see e. g.[8–9]

Within the mentioned class of reactions, one may well illustrate the influence of specific molecular parameters on the rate constants. The considered reactions are

$$CF_4\ (+M) \rightleftharpoons CF_3 + F\ (+M)\ \Delta H^\circ_0 = 541.7\ \text{kJ mol}^{-1} \quad \text{(R1)}$$

$$CF_3Cl\ (+M) \rightleftharpoons CF_3 + Cl\ (+M)\ \Delta H^\circ_0 = 361.0\ \text{kJ mol}^{-1} \quad \text{(R2)}$$

$$CF_3Br\ (+M) \rightleftharpoons CF_3 + Br\ (+M)\ \Delta H^\circ_0 = 292.8\ \text{kJ mol}^{-1} \quad \text{(R3)}$$

[a] *C. J. Cobos*
INIFTA, Facultad de Ciencias Exactas,
Universidad Nacional de La Plata, CONICET,
La Plata, Argentina
[b] *E. Tellbach, L. Sölter, J. Troe*
Max-Planck-Institut für Multidisziplinäre Naturwissenschaften,
Am Fassberg 11, D-37077 Göttingen,
Germany
and
Institut für Physikalische Chemie, Universität Göttingen,
Tammannstr. 6, D-37077 Göttingen,
Germany
E-mail: juergen.troe@mpinat.mpg.de

Supporting information for this article is available on the WWW under https://doi.org/10.1002/ijch.202300006

$$CF_3I\ (+M) \rightleftharpoons CF_3 + I\ (+M)\ \Delta H_0^\circ = 224.7\ \text{kJ mol}^{-1} \quad \text{(R4)}$$

Reactions R1–R4 have widely varying reaction enthalpies ΔH_0° and thus should show the influence of this quantity particularly well. The given values of ΔH_0° at 0 K are either from[10] or from the quantum-chemical calculations described below or in the Supporting Information, (SI; the values from the latter are used throughout the present calculations).

As the dissociation rate constants k_{dis} contain Boltzmann factors $\exp(-\Delta H_0^\circ/RT)$, their values may vary over many orders of magnitude. It, therefore, appears plausible to split off the Boltzmann factors and to analyze the remaining part of the rate constants. The analogous is achieved by focusing attention on recombination rate constants k_{rec}. As k_{dis} and k_{rec} are related by the equilibrium constant K_c through

$$K_c = k_{dis}/k_{rec}, \quad (1)$$

falloff curves of k_{rec} and of k_{dis} have the same shape and can be analyzed with respect to the dependence on molecular parameters in a similar manner (k_{dis} in s^{-1}, k_{rec} in $cm^3\,mol^{-1}\,s^{-1}$).

Falloff curves and, therefore, the kinetic order of the reaction with respect to the bath gas concentration [M], depend on the temperature T. This is first illustrated for reaction R1 in Figure 1 with modelled falloff curves for k_{rec} as a function of [Ar] and T. At 300 K and 1 bar of Ar (corresponding to [Ar] = 4×10^{-5} mol cm^{-3}), k_{rec} is predicted to be practically independent of [Ar]; i.e., the recombination is close to a second-order process. On the other hand, at 2000 K and 1 bar of Ar ([Ar] = 0.6×10^{-5} mol cm^{-3}), k_{rec} and, hence, also k_{dis} clearly depend on [Ar], such that the recombination is closer to a third-order process (while the dissociation R1 is closer to a second-order process). Obviously, it is essential to locate the falloff curves of the reaction at the considered conditions of pressure and temperature. Practical aspects of this procedure are the issue of the present article. An analysis of the described kind is often lacking in experimental work. Sometimes, a reaction order is assumed on intuition and the corresponding rate constant is used for arbitrary conditions. As this may introduce considerable errors, it does not appear acceptable. A complete analysis such as described in the following, therefore, has to be made.

2. Calculation of Rate Constants

The dominant quantities characterizing falloff curves like Figure 1 are the limiting high-pressure (subscript ∞) and low-pressure (subscript 0) rate constants. The transition between the limiting rate constants is also of importance, but matters less. In the following, we analyze the limiting rate constants first, before intermediate parts of the falloff curves are considered afterwards.

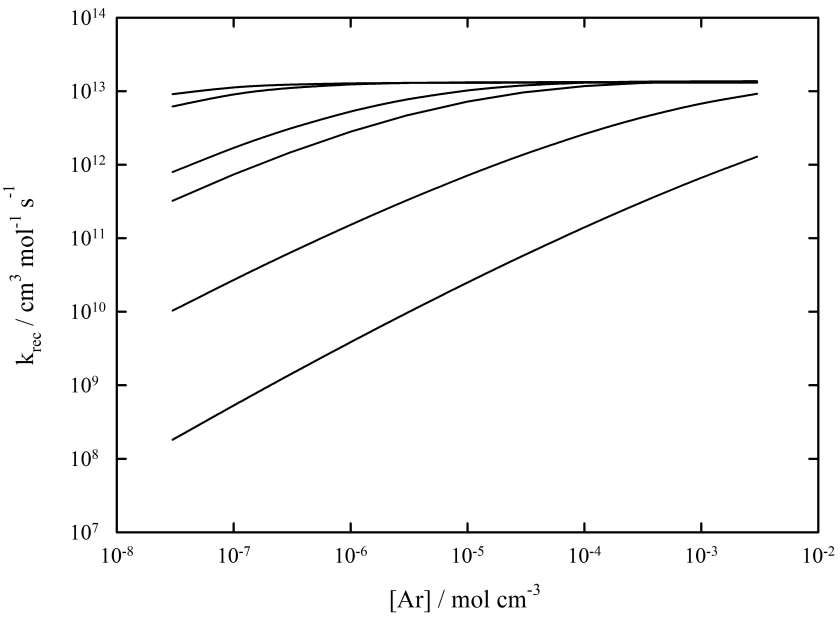

Figure 1. Falloff curves for the recombination reaction R1, i.e. $CF_3 + F\ (+Ar) \rightarrow CF_4\ (+Ar)$, at T = 300, 400, 800, 1000, 2000, and 4000 K (from top to bottom). Modelling results assuming values of $-\langle\Delta E\rangle_{total}/hc = 500$ cm^{-1} for collisional energy transfer (for the reason of this choice, see the text and the SI; modelled center broadening factors are F_{cent} = 0.76, 0.57, 0.26, 0.21, 0.12, and 0.12 for T = 300, 400, 800, 1000, 2000, 4000 K, respectively).

2.1 Quantum-Chemical Calculation of Molecular Properties

In this section, we examine relevant properties of the potential energy surfaces (PESs) of reactions R1–R4. All calculations were done at the G4 composite ab initio level of theory using the Gaussian 09 suite of programs[11] with the default integration grid,[12] while optimized molecular structures and harmonic vibrational frequencies were derived at the B3LYP/6-311+G(3df) level of density functional theory.[13]

In all cases, the electronic potential along the C–X-distance r of the reaction could well be fitted by a Morse potential

$$V(r) = D_e \{1-\exp[-\beta_e (r-r_e)]\}^2 \quad (2)$$

(for reaction R1 with the three parameters $D_e = 587\ kJ\,mol^{-1}$, $\beta_e = 1.66\ Å^{-1}$, and $r_e = 1.324$ Å, see the SI for the parameters of reactions R2–R4). Besides the electronic potential, also the anisotropy of the PES has to be characterized. This can be done by determining the r-dependence of the frequencies of the transitional modes, i.e. of those modes which change from vibrations into free rotations of the fragments relative to each other. Often, an exponential decay of the transitional mode frequencies was observed, such as described approximately by

$$\nu = \nu(r_e) \exp[-\alpha_e (r-r_e)] \quad (3)$$

For reaction R1 and its degenerate transitional mode, the parameters $\nu(r_e) = 516\ cm^{-1}$ and $\alpha_e = 0.89\ Å^{-1}$ were fitted such that $\alpha_e/\beta_e = 0.54$. A ratio of α_e/β_e much larger than unity would correspond to "loose activated complex" transition state theory (TST), i.e., to "phase space theory" (PST), whereas normal (and rigid) activated complex TST corresponds to smaller values of α_e/β_e.

The ratio of $\alpha_e/\beta_e = 0.54$ determined for reaction R1 is close to the average value of 0.5 found empirically for many simple bond dissociation processes in.[14] Table 1 compares a series of quantum-chemically determined ratios α_e/β_e (for reactions R1–R4 and recombination reactions with other C–F bonds). The shown values on average amount to $\alpha_e/\beta_e = 0.47 \pm 0.04$, indeed being close to 0.5, although some deviations are also observed.

Table 1. Modelled Morse- and anisotropy parameters, β_e and α_e, respectively (results derived by the described DFT- ab initio calculations).

Reaction	$\alpha_e/Å^{-1}$	$\beta_e/Å^{-1}$	α_e/β_e
CF_3+F	0.89	1.66	0.54
CF_3+Cl	0.75	1.65	0.46
CF_3+Br	0.69	1.60	0.43
CF_3+I	0.60	1.45	0.41
C_2F_5+F	0.53	1.76	0.30
$CF+F$	0.97	1.71	0.57
CF_2+F	1.74	2.90	0.60

Besides eqs. (2) and (3), also the dependence of the effective rotational constant $(B+C)/2$ of the reacting species along the minimum energy path (MEP) of the dissociating bond is of relevance. A fit in the form

$$(B+C)/2 = \{(B^*+C^*)/2\}\{1 + b_1 (r-r_e) + b_2 (r-r_e)^2\} \quad (4)$$

was found to be appropriate (for reaction R1 with the parameters $(B^*+C^*)/2 = 0.190\ cm^{-1}$, $b_1 = 0.374$, and $b_2 = 0.19$; r and r_e in Å; for reactions R2–R4, see the SI). Together with eqs. (2) and (3), eq. (4) serves for the determination of the minimum threshold energies $E_0(J)$ as a function of the total angular momentum (quantum number J), i.e. the centrifugal maxima of the PES. The $E_0(J)$ are required at various places of the calculations, for instance for the calculation of rate constants in the PST - limit. Eqs. (2)–(4) characterize those properties of the PES which enter the calculation of thermal rate constants in a dominant way, while finer details are mostly averaged out and appear only of minor importance.

2.2 Determination of Limiting High-Pressure Rate Constants

The high-pressure range of recombination corresponds to a capture situation where all encounters of reactants A and B lead to the formation of complexes AB to be stabilized by collisions. It, therefore, appears reasonable to express the limiting high-pressure recombination rate constants $k_{rec,\infty}$ in terms of simple hard-sphere collision theory, with rate constants k_{coll}^{HS} given by[15]

$$k_{coll}^{HS} = f_{el}\, d_{AB}^2\, (8\,\pi\, kT/\mu_{AB})^{1/2} \quad (5)$$

(with hard-sphere collision diameter d_{AB} and reduced mass μ_{AB} of the reactants A and B). An electronic weight factor $f_{el} = Q_{el}(AB)/Q_{el}(A)Q_{el}(B)$ with the respective electronic partition functions Q_{el} indicates which fraction of encounters leads into the relevant electronic state of AB. While k_{coll}^{HS} is well defined for a hard-sphere potential with contact distance d_{AB} between the reactants, the treatment changes for more complicated potentials like the Morse-potential of eq. (2). In this case, classical trajectory (CT) calculations allow one to determine rate constants k_{cap} for capture of the reactants. Systematic CT calculations have been made in[16] (for atoms combining with linear rotors) and[17] (for linear rotors combining with linear rotors) considering a variety of adduct geometries. The calculations led to approximate analytical expressions for a quantity defined by

$$Y(X) = k_{cap}^{PST}(8\,\pi\, kT/\mu_{AB})^{-1/2}\beta_e^2, \quad (6)$$

which corresponds to the ratio $k_{cap}^{PST}/k_{coll}^{HS}$ (f_{el} here is put equal to unity). The derived expressions were found to be of the form

$$Y(X) \approx a_0 + a_1 X + a_2 X^2 \quad (7)$$

with X defined by $X = \ln(kT/D_e) - \beta_e r_e$ and the coefficients determined as $a_0 = -15.7706$, $a_1 = -8.6364$, and $a_2 = 0.9975$ (often the equilibrium center-of-mass distance between the reactants A and B in the adduct AB may be used for r_e). It should be mentioned that accounting for the change of the rotational constant of the adduct along the MEP as described by eq. (4) has only a minor influence on eq. (7). On the other hand, the anisotropy of the potential described by eq. (3) reduces the capture rate constant k_{cap} to values smaller than k_{cap}^{PST}. We characterize this effect by a "rigidity factor" f_{rigid}, defined by

$$f_{rigid} = k_{rec,\infty}/k_{rec,\infty}^{PST} \quad (8)$$

As long as $f_{rigid} < 0.8$,

$$f_{rigid} \approx 8^{1/2}\ \{(B_e + C_e)/2\}\ D_e/\{h\nu(r_e)\}^2 \quad (9)$$

provides a useful approximation to the results of the CT calculations (for more detailed expressions, see[16] and[17]). One should also note that the results from the CT calculations coincide with results from the Statistical Adiabatic Channel Model (SACM)[18] such that the method is denoted by "SACM/CT". In the present work we have compared SACM/CT calculations of $k_{cap} = k_{rec,\infty}$ with $k_{cap}^{PST} = k_{rec,\infty}^{PST}$ (both from SACM/CT and classical PST calculations). Table 2 shows results for $k_{rec,\infty}^{PST}$, f_{rigid}, and $k_{rec,\infty} = f_{rigid}\ k_{rec,\infty}^{PST}$, for reactions R1–R4 and at temperatures between 300 and 4000 K. The various contributing molecular parameters (see the SI) according to eqs. (6)–(9) partly compensate each other such that specific trends are difficult to recognize.

Table 2. Modelled high-pressure recombination rate constants for reactions R1–R4 in phase space theoretical limit, $k_{rec,\infty}^{PST}$ (see text, upper third of the table, in 10^{12} cm^3 mol^{-1} s^{-1}), $k_{rec,\infty}$ (see text, lower third of the table, also in 10^{12} cm^3 mol^{-1} s^{-1}), and rigidity factors $f_{rigid} = k_{rec,\infty}/k_{rec,\infty}^{PST}$ (middle third of the table; the given f_{rigid} account for minor rotational contributions; f_{el} was included in all calculations).).

T/K	$CF_3 + F$	$CF_3 + Cl$	$CF_3 + Br$	$CF_3 + I$
		$k_{rec,\infty}^{PST}$		
300	67.6	54.9	47.6	41.7
1000	79.0	69.4	66.8	59.5
2000	87.0	75.8	80.7	71.5
4000	96.2	83.6	94.0	84.0
		f_{rigid}		
300	0.19	0.050	0.027	0.078
1000	0.17	0.055	0.032	0.11
2000	0.16	0.058	0.035	0.13
4000	0.15	0.061	0.038	0.15
		$k_{rec,\infty}$		
300	13.0	2.73	1.29	3.26
1000	13.7	3.80	2.13	6.37
2000	14.2	4.38	2.79	9.08
4000	14.6	5.07	3.52	12.6

In summary, we found that the calculated values of $k_{rec,\infty}$ generally agreed with the most probable experimental values within about a factor of two. As many parameters contribute to the high pressure rate constants, one cannot expect simple behavior, like simple temperature dependences.

2.3 Determination of Limiting Low-Pressure Rate Constants

After the calculation of limiting high-pressure rate constants $k_{rec,\infty}$ has been described in Section 2.2, limiting low-pressure rate constants $k_{rec,0}$ are considered in the following. By solving master equations for collisional activation/deactivation and assuming steady-state for the populations of excited states,[19] expressions for $k_{rec,0}$ could be represented in the form[20]

$$k_{rec,0} = [M]\ Z_{LJ}\ \beta_c\ \rho_{vib,h}(E_0)\ kT\ F_{anh}\ F_E\ F_{rot}\ [f_{el} f_{trans} f_{rot}/Q_{vib}(A)\ Q_{vib}(B)]. \quad (10)$$

Z_{LJ} here denotes the Lennard-Jones collision frequency between excited AB and M, $\rho_{vib,h}(E_0)$ is the harmonic vibrational density of states of excited AB at the dissociation energy $E_0 = E_0(J=0)$; F_{anh}, F_E, and F_{rot} are correction factors for anharmonicity, for the used expressions of the energy dependence of the vibrational density of states, and for rotation, respectively. f_{el} is as given above; f_{trans} and f_{rot} are the relevant ratios of translational and rotational partition functions in K_c; Q_{vib} and Q_{rot} are vibrational and rotational partition functions, respectively; The collision efficiency β_c is related to the average (total) energy $<\Delta E>_{total}$ transferred per collision through

$$\beta_c/(1-\beta_c^{1/2}) \approx -<\Delta E>_{total}/hc\ (F_E\ kT) \quad (11)$$

(one should note that $<\Delta E>_{total}$ is a negative quantity). For large values of the ratio $-<\Delta E>_{total}/hc$ (F_E kT), one has "strong collisions", i.e. β_c approaches unity. In the case $\beta_c < 1$, one speaks of "weak collisions".

The various molecular parameters enter the expression for $k_{rec,0}$ in an intricate manner. This is illustrated in Table 3, where some of the factors entering eq. (10) are compared for reactions R1–R4. The table shows that the decrease of $k_{rec,0}$/[Ar] from reaction R1 to reaction R4 is dominated by the decrease of $\rho_{vib,h}(E_0)$ which, in turn, is related to the decrease of E_0. As compact expressions for $\rho_{vib,h}(E_0)$ are available (see e.g.[21]), the trend of $k_{rec,0}$ within the considered group of reactions can well be quantified and be attributed mostly to the trend of $\rho_{vib,h}(E_0)$. At present, the largest uncertainty for the calculation of $k_{rec,0}$ appears to be the value of $<\Delta E>_{total}$ and, hence, of β_c. It is often used as an empirical fit parameter to be chosen of reasonable magnitude. However, theoretical calculations are also becoming possible (see e.g.[22]). Values of $-<\Delta E>_{total}/hc = 100$ cm^{-1} have been chosen for the calculations of Table 3, while an experimentally fitted value of 500 cm^{-1} was preferred in Figure 1 (further considerations are given below).

Table 3. Contributions to low-pressure rate constants $k_{rec,0}$ expressed by eq. (10) (modelling according to[20] for M = Ar and T = 300 K with E_0 in kJ mol^{-1}, Z_{LJ} in 10^{14} cm^3 mol^{-1} s^{-1}, $\rho_{vib,h}(E_0)$ in 10^8(kJ mol^{-1})$^{-1}$, and $k_{rec,0}$/[Ar] in 10^{20} cm^6 mol^{-2} s^{-1}; estimates of the collision efficiency β_c have been made through eq. (11) with $-<\Delta E>_{total}$/hc = 100 cm^{-1}).

	CF_3 + F (+Ar)	CF_3 + Cl (+Ar)	CF_3 + Br (+Ar)	CF_3 + I (+Ar)
E_0	542	361	293	225
Z_{LJ}	1.7	1.8	1.8	1.8
$\rho_{vib,h}(E_0)$	7.5	1.4	0.68	0.15
F_{anh}	1.8	1.2	1.2	1.2
F_E	1.04	1.05	1.06	1.08
F_{rot}	15.5	16.2	19.1	16.6
β_c	0.24	0.24	0.23	0.23
$k_{rec,0}$/[Ar]	9.7	5.4	2.5	0.49

2.4 Falloff Curves

The calculation of the limiting high- and low-pressure rate constants ($k_{rec,\infty}$ or $k_{dis,\infty}$ and $k_{rec,0}$ or $k_{dis,0}$) by eqs. (5)–(11) allows one to locate the position of the falloff curves along the scale of bath gas concentrations [M]. The most important quantity in this respect is that value of [M], denoted by $[M]_{cent}$, for which the extrapolated $k_{rec,0}$ ([M]) (or $k_{dis,0}$ ([M])) is equal to $k_{rec,\infty}$ (or $k_{dis,\infty}$); i. e., $[M]_{cent}$ is defined by

$$[M]_{cent} = k_{rec,0}/k_{rec,\infty} = k_{dis,0}/k_{dis,\infty}. \quad (12)$$

The results described in sections 2.2 and 2.3 lead to important conclusions on $[M]_{cent}$. First, one notes that $[M]_{cent}$ markedly increases with increasing temperature. This is illustrated, e. g., in Figure 1 where $[Ar]_{cent}$ increases from $[Ar]_{cent} \approx 2\times10^{-11}$ mol cm^{-3} at 300 K to $[Ar]_{cent} \approx 2\times10^{-4}$ mol cm^{-3} at 3000 K. Second, one observes some dependence on the chosen value of $<\Delta E>_{total}$. E. g., at 3000 K one has $[Ar]_{cent} \approx 7\times10^{-4}$ mol cm^{-3} for $-<\Delta E>_{total}$/hc = 100 cm^{-1} while $[Ar]_{cent} \approx 7\times10^{-5}$ mol cm^{-3} for $-<\Delta E>_{total}$/hc = 2000 cm^{-1}.

While the value of $[M]_{cent}$ is of central importance, one also has to consider the shape of the falloff curves, i. e. the type of transition from $k_{rec,0}$ to $k_{rec,\infty}$ (or from $k_{dis,0}$ to $k_{dis,\infty}$). In the simple Lindemann-Hinshelwood model of competing single-step inter- and intra- molecular processes, it would be given by

$$k_{rec}/k_{rec,\infty} = x/(1+x) \quad (13)$$

where $x = k_{rec,0}/k_{rec,\infty}$ or $x = k_{dis,0}/k_{dis,\infty}$ The results of more detailed treatments, like the RRKM (Rice – Ramsperger–Kassel – Marcus) model, however, require modifications of this result. These may be represented by an additional "broadening factor" $F(x)$ to be multiplied with the right-hand side of eq. (13).[23] $F(x)$ can be interpreted in terms of an "effective number of oscillators" of the system, and it can be estimated for strong collisions (superscript sc) as well as weak collisions (superscript wc). One has $F(x) \approx F(x)^{sc}\ F(x)^{wc}$ where $F(x)^{sc}$ can be estimated with the methods of[23] while $F(x)^{wc}$ can be expressed by the collision efficiency β_c.[20,24,25]

Most importantly, $F(x)$ is characterized by a "central broadening factor", defined by $F_{cent} = F(x=1)$. With this value, $F(x)$ can roughly be approximated by[20]

$$\log F(x) \approx \{1/[1+(\log x/N)^2]\}\ \log F_{cent} \quad (14)$$

where

$$N \approx 0.75 - 1.27 \log F_{cent} \quad (15)$$

In case of very broad falloff curves (small F_{cent}), a more refined, alternative, expression has been proposed in [24, 25]. It is of the form

$$F(x) = (1+x/x_0)/[\,1+(x/x_0)^n]^{1/n} \quad (16)$$

where x_0 has been found in the range 0.9–1. N is related to F_{cent} by

$$n = [\ln 2/\ln(2/F_{cent})]\ [1-b+b\ (x/x_0)^q] \quad (17)$$

where $q = (F_{cent}-1)/\ln(F_{cent}/10)$ and b has been found in the range 0.1–0.25. For simplicity, we mostly used $x_0 = 1$ and b = 0.2.

Using $-<\Delta E>_{total}$/hc = 500 cm^{-1} (see the following section), sets of falloff curves for the recombination reactions R2–R4 have been calculated. Figures 2–4 show the results. The shapes of the curves are all quite similar to that shown in Figure 1 for reaction R1. However, because of different $[Ar]_{cent}$ (mostly caused by different $\rho_{vib,h}(E_0)$, due to different E_0), the position of the curves along the scale of [Ar] are different. In practice it matters more that the reactions in the dissociation direction are studied at different temperatures. Reaction R1 in the dissociation direction, e. g., in our laboratory has been studied at temperatures around 2500 K,[26] while the corresponding dissociation experiments for reaction R4 have been made at half that temperature.[27–29]

3. Practical Problems

The dependence of the reaction order on the nature of the bath gas M and on the temperature T, such as illustrated in Figures 1–4, poses a challenge to applications. In order to determine the reaction order, one either has to perform experiments over a sufficiently broad pressure range, which may be difficult to do, or one may try to compare measurements with modelled falloff curves, which is hampered by uncertainties in the input quantities (to a small extent of the reaction enthalpy ΔH°_0 and to a much larger extent of the energy transfer parameter $<\Delta E>_{total}$). Further difficulties may arise when the composition of the bath gas, during an

Israel Journal of Chemistry

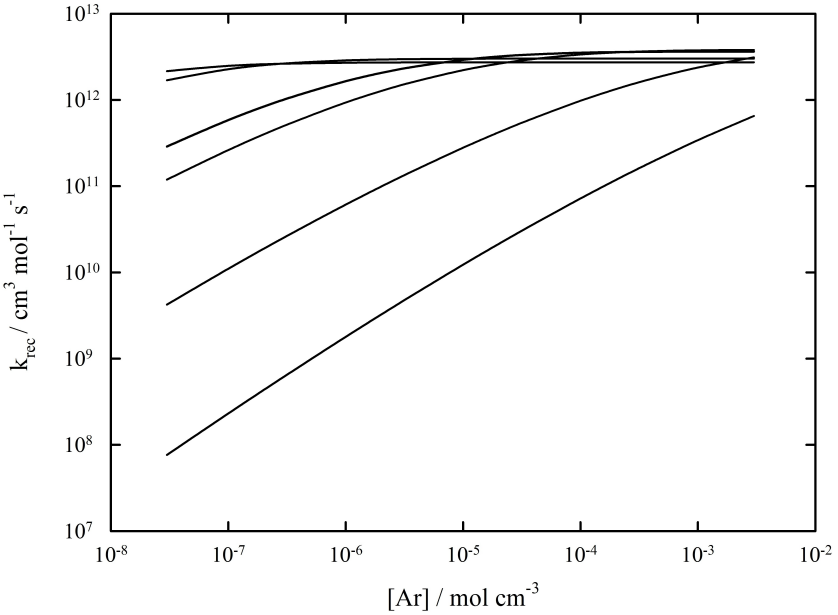

Figure 2. Falloff curves for the recombination reaction R2, $CF_3 + Cl$ (+Ar)→CF_3Cl (+Ar), at $T = 300$, 400, 800, 1000, 2000, and 4000 K (from top to bottom). Modelling results assuming values of $-<\Delta E>_{total}/hc = 500\ cm^{-1}$ for collisional energy transfer (see text and the SI; modelled center broadening factors are $F_{cent} = 0.65$, 0.49, 0.23, 0.18, 0.12, and 0.16 for $T = 300$, 400, 800, 1000, 2000, 4000 K, respectively).

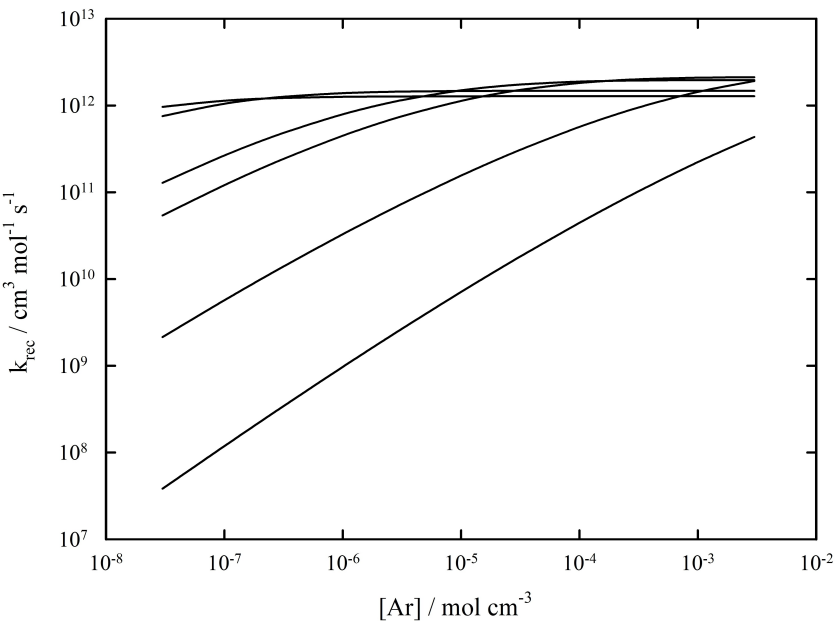

Figure 3. Falloff curves for the recombination reaction R3, $CF_3 + Br$ (+Ar)→CF_3Br (+Ar), at $T = 300$, 400, 800, 1000, 2000, and 4000 K (from top to bottom). Modelling results assuming values of $-<\Delta E>_{total}/hc = 500\ cm^{-1}$ for collisional energy transfer (see text and the SI; modelled center broadening factors are $F_{cent} = 0.59$, 0.44, 0.21, 0.18, 0.14, and 0.20 for $T = 300$, 400, 800, 1000, 2000, 4000 K, respectively).

experiment, changes with time. The effects of uncertainties in ΔH°_0 and $<\Delta E>_{total}$ may be difficult to disentangle (the value of $<\Delta E>_{total}/hc = -500\ cm^{-1}$ used in the modelling of Figures 1–4 has been taken from the analysis[30] of dissociation experiments of CF_4 in Ar near 2500 K,[26] assuming an only weak temperature dependence of $<\Delta E>_{total}$, see[31]).

The situation looks simplest for recombination experiments near room temperature. For bath gas pressures near to 1 Torr (corresponding to $[M] \approx 5 \times 10^{-8}\ mol\,cm^{-3}$), Figures 1–4 indicate that k_{rec} for all reactions R1–R4 is close to their high-pressure second-order limit. Replacing M = Ar by M = He changes the situation only slightly. Nevertheless, a small drop

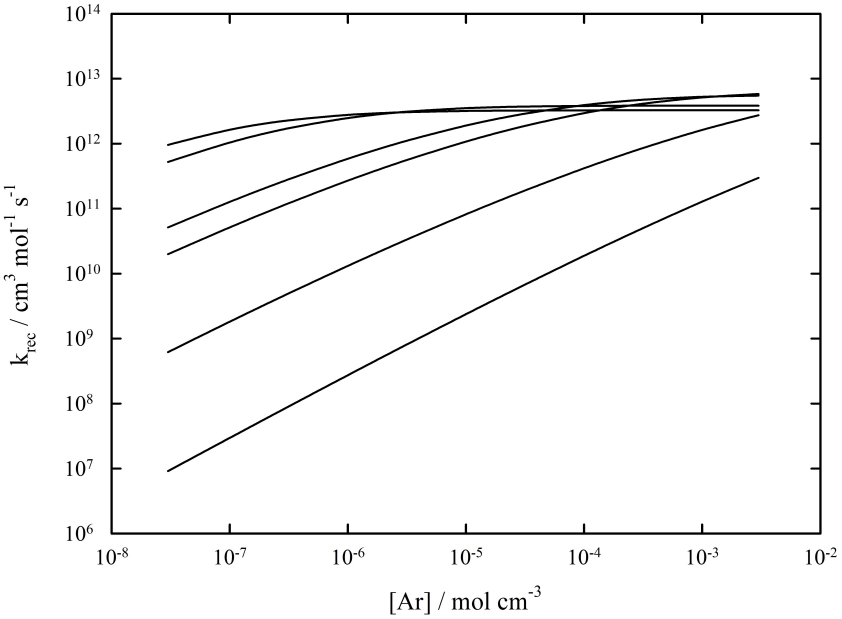

Figure 4. Falloff curves for the recombination reaction R4, $CF_3 + I\ (+Ar) \rightarrow CF_3I\ (+Ar)$, at $T = 300$, 400, 800, 1000, 2000, and 4000 K (from top to bottom). Modelling results assuming values of $-<\Delta E>_{total}/hc = 500\ cm^{-1}$ for collisional energy transfer (see text and the SI; modelled center broadening factors are $F_{cent} = 0.56$, 0.43, 0.22, 0.19, 0.18, and 0.26 for $T = 300$, 400, 800, 1000, 2000, 4000 K, respectively).

of k_{rec} with decreasing [He] for reaction R1 was reported in [8]. It was shown in [30] that this is compatible with modelling results. On the other hand, the stronger dependences of k_{rec} on [M] reported in[32][33] appear less probable and call for a re-analysis of the experiments. A representation as a third-order process certainly does not appear justified. Studies of the thermal dissociation of CF_4 at temperatures between 2000 and 3000 K and [Ar] between 5×10^{-6} and 10^{-4} mol cm^{-3} in [26, 34], according to Figure 1 locate the reaction between a second-order and a first-order process. The analogous applies to dissociation experiments for CF_3Cl.[35] For the dissociation of CF_3Br (see e. g. [35–37]), and even more that of CF_3I,[27–29,35] the intermediate reaction order had to be accounted for. A representation as a first-order process here did not appear justified at all. Instead, rate constants k_{dis} had to be reported for a fixed pressure (or [M]) such as done in [6], or full falloff curves have to be determined and rate constants represented accordingly. Experimental and modelling studies of the thermal dissociations of CF_3Cl, CF_3Br, and CF_3I at low bath gas pressures (corresponding to 10^{-6} mol cm^{-3}) have all been represented as second-order processes. While this appears realistic for the temperatures near 2000 K as applied in the studies of CF_3Cl and CF_3Br, for the lower temperatures (near 1000 K) employed for the dissociation of CF_3I, deviations due to the transition to first-order behavior according to Figure 4 have to be expected. A re-analysis of the available results with full falloff curves thus appears advisable.

In any case, it is not possible to model dissociation pathways of SF_6-alternatives like perfluoroketones or perfluoronitriles by sequences of first-order processes characterized by simple Arrhenius expressions of their rate constants. It may be more appropriate to assume second-order dissociation behavior with effective rate constants taken from falloff curves at the relevant pressures. The falloff curves for k_{rec} shown in Figures 1–4 may serve for this purpose.

Acknowledgements

The authors are grateful to Professor Helmut Schwarz for his long-standing encouragement of kinetic work and his inspiring suggestions of applications. Support by the Deutsche Forschungsgemeinschaft (Project TR69/21-3) is also gratefully acknowledged. Open Access funding enabled and organized by Projekt DEAL.

Data Availability Statement

The data that support the findings of this study are available from the corresponding author upon reasonable request.

References

[1] *"Faraday Discussions Vol. 238: Unimolecular Reactions"* (Oxford, U.K., 22–24 June **2022**, Royal Society of Chemistry).
[2] D. L. Baulch, C. T. Bowman, C. J. Cobos, R. A. Cox, T. Just, J. A. Kerr, M. J. Pilling, D. Stocker, J. Troe, W. Tsang, R. W. Walker, J. Warnatz, *J. Phys. Chem. Ref. Data* **2005**, *34*, 757–1397.

[3] A. Mellouki, M. Ammann, R. A. Cox, J. N. Crowley, H. Herrmann, M. E. Jenkin, V. F. McNeill, J. Troe, T. J. Wallington, *Atm. Chem. Phys.* **2021**, *21*, 4797–4808.
[4] V. Wakelam, E. Herbst, J. C. Loison, I. W. M. Smith, V. Chandrasekaran, B. Pavone, N. G. Adams, M. C. Bacchus-Montabonel, A. Bergeat, K. Beroff, V. M. Bierbaum, M. Chabot, A. Dalgarno, E. F. van Dishoeck, A. Faure, W. D. Geppert, D. Gerlich, D. Galli, E. Hebrard, F. Hersant, K. M. Hickson, P. Honvault, S. J. Klippenstein, S. Le Picard, G. Nyman, P. Pernot, S. Schlemmer, F. Selsis, I. R. Sims, D. Talbi, J. Tennyson, J. Troe, R. Wester, L. Wiesenfeld, *Astrophys. J. Suppl. Ser.* **2012**, *199–21*, 1–10.
[5] Y. Wu, C. Wang, H. Sun, A. B. Marphy, M. Rong, F. Yang, Z. Chen, C. Niu, *J. Phys. D* **2018**, *51*, 155206.
[6] L. Chen, B. Zhang, X. Li, *J. Phys. D* **2020**, *53*, 415502.
[7] B. Zhang, J. Xiong, L. Chen, X. Li, A. B. Murphy, *J. Phys. D* **2020**, *53*, 173001.
[8] I. C. Plumb, K. R. Ryan, *Plasma Chem. Plasma Process.* **1986**, *6*, 11–25.
[9] I. C. Plumb, K. R. Ryan, *Plasma Chem. Plasma Process.* **1986**, *6*, 205–230.
[10] J. B. Burkholder, S. P. Sander, J. Abbatt, J. R. Barker, C. Cappa, J. D. Crounse, T. S. Dibble, R. E. Huie, C. E. Kolb, M. J. Kurylo, V. L. Orkin, C. J. Percival, D. M. Wilmouth, P. H. Wine. *JPL Publication 19–5. Evaluation no. 19*, **2020** Jet Propulsion Laboratory, Pasadena (http://jpldataeval.jpl.nasa.gov).
[11] M. J. Frisch, G. W. Trucks, H. B. Schlegel, G. E. Scuseria, M. A. Robb, J. R. Cheeseman, G. Scalmani, V. Barone, B. Mennucci, G. A. Petersson, H. Nakatsuji, M. Caricato, X. Li, H. P. Hratchian, A. F. Izmaylov, J. Bloino, G. Zheng, J. L. Sonnenberg, M. Hada, M. Ehara, K. Toyota, R. Fukuda, J. Hasegawa, M. Ishida, T. Nakajima, Y. Honda, O. Kitao, H. Nakai, T. Vreven, J. A. Montgomery, J. E. Peralta, F. Ogliaro, M. Bearpark, J. J. Heyd, E. Brothers, K. N. Kudin, V. N. Staroverov, R. Kobayashi, J. Normand, K. Raghavachari, A. Rendell, J. C. Burant, S. S. Iyengar, J. Tomasi, M. Cossi, M. Rega, M. Klene, J. E. Knox, J. B. Cross, V. Bakken, C. Adamo, J. Jaramillo, R. E. Gomperts, O. Stratmann, A. J. Yazyev, R. Austin, C. Cammi, J. W. Pomelli, R. Ochterski, R. L. Martin, K. Morokuma, V. G. Zakrzewski, G. A. Voth, P. Salvador, J. J. Dannenberg, S. Dapprich, A. D. Daniels, O. Farkas, J. B. Foresman, J. V. Ortiz, J. Cioslowski, D. J. Fox, Gaussian, *" Gaussian 09"*, **2009**,Wallingford, CT.
[12] L. A. Curtiss, P. C. Redfern, K. Raghavachari, *J. Chem. Phys.* **2007**, *126*, 084108.
[13] A. D. Becke, *Phys. Rev. A* **1988**, *38*, 3098–3100.
[14] C. J. Cobos, J. Troe, *J. Chem. Phys.* **1985**, 1010–1015.
[15] H. S. Johnston (*"*Gas phase reaction rate theory*"*. The Ronald Press Company, New York, **1966**).
[16] A. I. Maergoiz, E. E. Nikitin, J. Troe, V. G. Ushakov, *J. Chem. Phys.* **1998**, *108*, 5265–5280.
[17] A. I. Maergoiz, E. E. Nikitin, J. Troe, V. G. Ushakov, *J. Chem. Phys.* **1998**, *108*, 9987–9998.
[18] M. Quack, J. Troe, *Ber. Bunsenges. Phys. Chem.* **1974**, *78*, 240–252.
[19] J. Troe, *J. Chem. Phys.* **1977**, *66*, 4745–4757.
[20] J. Troe, *J. Phys. Chem.* **1979**, *83*, 114–128.
[21] G. Z. Whitten, B. S. Rabinovitch, *J. Chem. Phys.* **1963**, *38*, 2466–2473.
[22] A. W. Jasper, C. M. Oana, J. A. Miller, *Proc. Combust. Inst.* **2015**, *35*, 197–204.
[23] J. Troe, *Ber. Bunsenges. Phys. Chem.* **1974**, *78*, 478–488.
[24] J. Troe, V. G. Ushakov, *J. Chem. Phys.* **2011**, *135*, 054304.
[25] J. Troe, V. G. Ushakov, *Z. Phys. Chem.* **2014**, *228*, 1–10.
[26] G. Knight, L. Sölter, E. Tellbach, J. Troe, *Phys. Chem. Chem. Phys.* **2016**, *16*, 17592–17596.
[27] S. S. Kumaran, M.–C. Su, K. P. Lim, J. V. Michael, *Chem. Phys. Lett.* **1995**, *243*, 59–63.
[28] N. S. Bystrov, A. V. Emilianov, A. V. Eremin, P. I. Yatsenko, *J. Phys. D* **2018**, *51*, 184004.
[29] C. J. Cobos, L. Sölter, E. Tellbach, J. Troe, *Phys. Chem. Chem. Phys.* **2019**, *21*, 23893–23899.
[30] C. J. Cobos, L. Sölter, E. Tellbach, J. Troe, *J. Phys. Chem. A* **2023**, *127*, 1697-1701.
[31] C. J. Cobos, J. Troe, *Z. Phys. Chem.* **1992**, *176*, 161–171.
[32] N. I. Butkovskaya, M. N. Larichev, I. O. Leipunskii, I. I. Morosov, V. I. Talroze, *Kinet. Catal.* **1980**, *21*, 263–267.
[33] B. Dils, J. Vertommen, S. A. Carl, L. Vereecken, J. Peeters, *Phys. Chem. Chem. Phys.* **2005**, *7*, 1187–1193.
[34] A. P. Modica, S. J. Sillers, *J. Chem. Phys.* **1968**, *48*, 3283–3289.
[35] J. H. Kiefer, R. Sathyanarayana, *Int. J. Chem. Kinet.* **1997**, *29*, 705–716.
[36] W. Tsang, *J. Phys. Chem.* **1986**, *90,* 414–418.
[37] I. Hranisavljevic, J. J. Carroll, M.–C. Su, J. V. Michael, *Int. J. Chem. Kinet.* **1998**, *30*, 859–867.

Manuscript received: January 16, 2023
Revised manuscript received: February 22, 2023
Version of record online: March 14, 2023